Quasiequatorial gravitational lensing by spinning black holes in the strong field limit

V. Bozza*
Centro Studi e Ricerche "Enrico Fermi," Rome, Italy,
Dipartimento di Fisica "E.R. Caianiello," Università di Salerno, Salerno, Italy,
and Istituto Nazionale di Fisica Nucleare, Sezione di Napoli, Napoli, Italy
(Received 31 October 2002; published 22 May 2003)

Spherically symmetric black holes produce, by strong field lensing, two infinite series of relativistic images, formed by light rays winding around the black hole at distances comparable to the gravitational radius. In this paper we address the relevance of the black hole spin for the strong field lensing phenomenology, focusing on trajectories close to the equatorial plane for simplicity. In this approximation, we derive a two-dimensional lens equation and formulas for the position and the magnification of the relativistic images in the strong field limit. The most outstanding effect is the generation of a nontrivial caustic structure. Caustics drift away from the optical axis and acquire finite extension. For a high enough black hole spin, depending on the source extension, we can practically observe only one image rather than two infinite series of relativistic images. In this regime, additional nonequatorial images may play an important role in the phenomenology.

DOI: 10.1103/PhysRevD.67.103006 PACS number(s): 95.30.Sf, 04.70.Bw, 98.62.Sb

I. INTRODUCTION

Gravitational lensing, since its beginning, has been used to test general relativity in the weak field approximation. Later on, several studies of null geodesics in strong gravitational fields were made. Bardeen *et al.* [1] studied the appearance of a black hole in front of a uniform source; Viergutz [2] made a semianalytical investigation of null geodesics in Kerr geometry; Nemiroff [3] studied the visual distortions around a neutron star and around a black hole; Falcke, Melia and Agol [4] considered the luminosity of the accretion flow as a source.

A recent paper by Virbhadra and Ellis [5] has aroused new interest about gravitational lensing as a probe for strong gravitational fields generated by collapsed objects, providing a new important test for the full general relativity. They have shown that a source behind a Schwarzschild black hole could generate an infinite series of images on both sides of the lens. These relativistic images are formed by light rays passing close to the event horizon and winding several times around the black hole before emerging towards the observer. By an alternative formulation, Frittelli, Kling and Newman [6] attained an exact lens equation, giving integral expressions for its solutions, and compared their results to those by Virbhadra and Ellis. The phenomenology of collapsed objects with naked singularities, analyzed by Virbhadra and Ellis in another work [7], is radically different. This difference provides a possible way to test the correctness of the cosmic censorship conjecture.

A new, simple and reliable method to investigate the subject was proposed by Bozza *et al.* in Ref. [8]. They reexamined the Schwarzschild black hole lensing defining a *strong field limit* for the deflection angle, which retained the first two leading order terms. By this approximation, a fully analytical treatment was developed and simple formulas for the position and the magnification of the images were derived. The same method was applied by Eiroa, Romero and Torres [9] to a Reissner-Nordström black hole, confirming the appearance of a similar pattern of images. Later on, the formulas given in Ref. [8] were used by Petters [10] to calculate relativistic effects on microlensing events. Finally, in a previous work, we have developed a generalization of the strong field limit to an arbitrary spherically symmetric spacetime [11], comparing the image patterns for several interesting metrics. We have shown that different collapsed objects are distinguishable by a careful examination of the separation between the first two relativistic images and their luminosity ratio. The sensitivities required for such measures are out of the actual very long baseline interferometry (VLBI) projects [12], but might be reached in a not so far future.

Insofar, only spherically symmetric black holes have been adequately investigated. Yet, in general, a black hole would be characterized by a non-zero intrinsic angular momentum which breaks spherical symmetry, leaving only a rotational symmetry around one axis. Rotation heavily affects the gravitational field around the collapsed object. It is thus natural to expect relevant modifications in the phenomenology of strong field gravitational lensing.

A further motivation for such a study comes from the fact that previous works on the subject have selected the supermassive black hole hosted by the radio source Sagittarius A* [13] as the best candidate for strong field gravitational lensing [5,11]. Its mass has been estimated to be $M=2.6\times10^6 M_\odot$ but our knowledge on a possible intrinsic angular momentum of this object is still very poor. However, the analysis of the variability of the spectrum in the millimeter-submillimeter region suggests the possibility of a non-negligible spin [14]. In particular, the value

$$|a|\approx 0.044 \tag{1}$$

has been proposed (with respect to Ref. [14], we normalize distances to the Schwarzschild radius rather than to the black hole mass, hence the factor 1/2 in this value), but high

*Electronic address: valboz@sa.infn.it

uncertainties in the assumptions behind the calculations may push the spin towards even higher values.

The purpose of this paper is to investigate the relevance of the black hole spin in strong field lensing phenomenology. We formulate the strong field limit for Kerr black hole lensing, considering trajectories close to the equatorial plane. With this limitation we cannot give a complete description of the whole phenomenology, which we shall delay to future works. However, as we shall see, quasi-equatorial motion yields very sharp indications useful to understand also the general case. In particular, we will show that the presence of a sufficiently high black hole spin drastically changes the expected pattern of observable images.

This paper is structured as follows. In Sec. II we recall some general properties of Kerr geodesics. In Sec. III we carry out the strong field limit expansion of the deflection angle on the equatorial plane. In Sec. IV we move off from the equatorial plane and consider trajectories at small declinations. In Sec. V we write the lens equation on the equatorial plane. In Sec. VI we write a polar lens equation dealing with displacements normal to the equatorial plane. In Sec. VII we find the positions of the caustic points and the magnification of all images in the equatorial plane. In Sec. VIII we describe the critical curves and caustic structure. Section IX discusses the effects of the black hole spin on the gravitational lensing phenomenology, with special reference to the black hole at the center of our Galaxy. Section X contains the summary.

II. GEODESICS IN KERR SPACETIME

In Boyer-Lindquist coordinates [15] $x^\mu \equiv (t,x,\vartheta,\phi)$, the Kerr metric reads

$$ds^2 = \frac{\Delta - a^2\sin^2\vartheta}{\rho^2}dt^2 - \frac{\rho^2}{\Delta}dx^2 - \rho^2 d\vartheta^2 - \frac{(x^2+a^2)^2 - a^2\Delta\sin^2\vartheta}{\rho^2}\sin^2\vartheta d\phi^2 + \frac{2ax\sin^2\vartheta}{\rho^2}dt d\phi \tag{2}$$

$$\Delta = x^2 - x + a^2 \tag{3}$$

$$\rho^2 = x^2 + a^2\cos^2\vartheta \tag{4}$$

where a is the specific angular momentum of the black hole. All distances are measured in Schwarzschild radii ($2MG/c^2=1$).

The Kerr space is characterized by a spherical event horizon at $x_H = (1+\sqrt{1-4a^2})/2$ for $|a|<0.5$. Beyond this critical value of the spin there is no event horizon and causality violations are present in the whole spacetime, with the appearance of a naked singularity [16,17]. We shall restrict to subcritical angular momenta. The ellipsoid $\Delta - a^2\sin^2\vartheta = 0$ is the static limit bounding the region where every static worldine ($x=\vartheta=\phi=0$) becomes spacelike. The region between the static limit and the horizon is called ergosphere: here everything is bound to rotate around the black hole.

The geodesics equations can be derived taking

$$\mathcal{L} = g_{\mu\nu}\dot{x}^\mu\dot{x}^\nu \tag{5}$$

as the Lagrangian, where the dot indicates the derivative with respect to some affine parameter.

Finding four integrals of motion, we can transform these equations into a set of four first order equations which are equivalent to the original ones. Two constants of motions are the energy and the angular momentum of the particle, given by

$$2E = \frac{\partial\mathcal{L}}{\partial\dot{t}} \tag{6}$$

$$-2J = \frac{\partial\mathcal{L}}{\partial\dot{\phi}}. \tag{7}$$

By a suitable choice of the affine parameter, we can set

$$E = 1. \tag{8}$$

From these equations, we find an expression for $\dot{t}$ and $\dot{\phi}$ in terms of x, ϑ and J

$$\dot{t} = \frac{g_{33} + g_{03}J}{g_{33}g_{00} - g_{03}^2} \tag{9}$$

$$\dot{\phi} = \frac{g_{00}J + g_{03}}{g_{03}^2 - g_{33}g_{tt}}. \tag{10}$$

$\mathcal{L}$ is another constant of motion, which vanishes for null geodesics and can be used to write $\dot{x}$

$$\dot{x} = \pm\sqrt{\frac{-g_{00}\dot{t}^2 - g_{22}\dot{\vartheta}^2 - g_{33}\dot{\phi}^2 - 2g_{03}\dot{t}\dot{\phi}}{g_{11}}}. \tag{11}$$

Finally, $\dot{\vartheta}$ can be obtained in terms of a fourth integral of motion, separating the Hamilton-Jacobi equation [16]:

$$\dot{\vartheta} = \pm\frac{1}{\rho^2}\sqrt{Q + a^2\cos^2\vartheta - J^2\cot^2\vartheta}. \tag{12}$$

Equations (9)–(12) represent the sought set of first order differential equations, suitable for a detailed study.

The integrals of motion J and Q can be expressed in terms of the geometric parameters of the incoming light ray trajectory. In general, we can identify a light ray coming from infinity by three parameters (Fig. 1), referring to the straight line which the photon would follow if there were no gravitational field. The projection of this line on the equatorial plane has a distance u from the origin, which we shall call the projected impact parameter. At this minimum projected distance, the light ray has some height h on the equatorial plane. Finally, the inclination ψ_0 is the angle that the light ray forms with the equatorial plane. When we switch on the

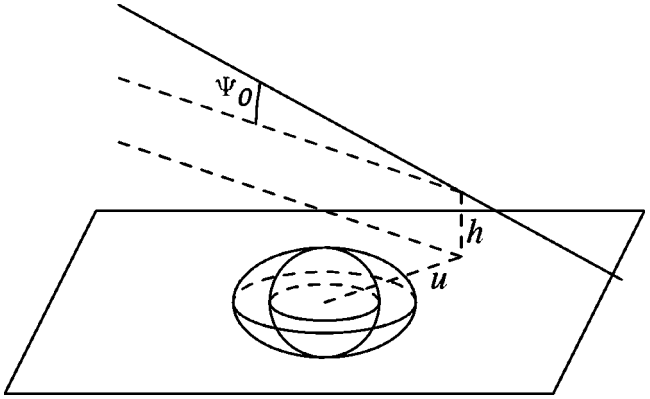

FIG. 1. The three parameters identifying an incoming light ray.

gravitational field, the light ray is obviously deviated from this ideal straight line, but these three parameters can still be used to label any light rays coming from infinity. Taking the asymptotic limit of the equations of motion, we can write J and Q in terms of the initial conditions characterizing the light ray

$$J = u\cos\psi_0 \tag{13}$$

$$Q = h^2\cos^2\psi_0 + (u^2 - a^2)\sin^2\psi_0 . \tag{14}$$

III. DEFLECTION ANGLE IN THE EQUATORIAL PLANE

In this section we consider light rays strictly lying on the equatorial plane $\vartheta = \pi/2$ by setting $h = \psi_0 = 0$. The reduced metric has the form

$$ds^2 = A(x)dt^2 - B(x)dx^2 - C(x)d\phi^2 + D(x)dtd\phi \tag{15}$$

with

$$\begin{aligned} A(x) &= 1 - \frac{1}{x} \\ B(x) &= \frac{1}{1 - \frac{1}{x} + \frac{a^2}{x^2}} \\ C(x) &= x^2 + a^2 + \frac{a^2}{x} \\ D(x) &= 2\frac{a}{x}. \end{aligned} \tag{16}$$

What we say in this section is immediately extendable to any axially symmetric spacetime if we replace Eq. (16) by any other expression.

As $\psi_0 = 0$, by Eq. (13) the angular momentum J coincides with the impact parameter u. The impact parameter is also related to the minimum distance x_0 reached by the photon. In general, a light ray coming from infinity approaches the black hole, reaches this minimum distance x_0 and then leaves again towards infinity. Evaluating the Lagrangian at $x = x_0$, we find an implicit relation between $J = u$ and the closest approach distance x_0:

$$\begin{aligned} J = u &= \frac{-D_0 + \sqrt{4A_0C_0 + D_0^2}}{2A_0} \\ &= \frac{-a + x_0\sqrt{a^2 + x_0(x_0 - 1)}}{x_0 - 1}, \end{aligned} \tag{17}$$

where all the metric functions with the subscript 0 are evaluated at $x = x_0$. The impact parameter u is then univocally determined by x_0 and vice versa. Choosing the positive sign before the square root, we describe only light rays winding counterclockwise when seen from above. For $a > 0$ the black hole also rotates counterclockwise, while for $a < 0$ the black hole and the photon rotate in opposite senses.

Dividing $\dot{\phi}$ by $\dot{x}$, we find the azimuthal shift as a function of the distance

$$\frac{d\phi}{dx} = P_1(x, x_0)P_2(x, x_0) \tag{18}$$

$$P_1(x, x_0) = \frac{\sqrt{B}(2A_0AJ + A_0D)}{\sqrt{CA_0}\sqrt{4AC + D^2}} \tag{19}$$

$$P_2(x, x_0) = \frac{1}{\sqrt{A_0 - A\frac{C_0}{C} + \frac{J}{C}(AD_0 - A_0D)}}. \tag{20}$$

Integrating this expression from x_0 to infinity we find half the deflection angle as a function of the closest approach. Given the symmetry between approach and departure, we can write the whole deflection angle as

$$\alpha(x_0) = \phi_f(x_0) - \pi \tag{21}$$

$$\phi_f(x_0) = 2\int_{x_0}^{\infty} \frac{d\phi}{dx} dx. \tag{22}$$

$\phi_f(x_0)$ is the total azimuthal shift. It evaluates to π for a straight line and becomes larger as the light ray is bent by the gravitational field. The expression for a spherically symmetric metric, given in Ref. [11] can be recovered setting $D = D_0 = 0$.

The deflection angle grows as x_0 decreases. It diverges when x_0 reaches a minimum value x_m which represents the radius of the photon sphere. If a photon falls inside this sphere, it is destined to be absorbed by the black hole. Of course, we will have different photon spheres for photons winding in the same sense of the rotation of the black hole (hereafter direct photons) and for photons winding in the opposite sense (retrograde photons). In general, we expect the latter to be absorbed more easily. Their photon sphere will thus be larger than that of retrograde photons, which can escape more easily. As we shall see later, this is what happens.

Following the philosophy of the strong field limit, we look for an expansion of the deflection angle of the form

$$\alpha(\theta) = -\bar{a}\log\left(\frac{\theta D_{OL}}{u_m} - 1\right) + \bar{b} + O(u - u_m) \tag{23}$$

where the coefficients u_m, $\bar{a}$ and $\bar{b}$ depend on the metric functions evaluated at x_m. D_{OL} is the distance between the lens and the observer, so that the angular separation of the image from the lens (also referred as impact angle) is $\theta = u/D_{OL}$.

All the steps to be taken towards this final expression are very similar to those for spherically symmetric black holes, with few adjustments. We shall sketch them very briefly, referring to Ref. [11] for details.

We define the variables

$$y = A(x) \tag{24}$$

$$z = \frac{y - y_0}{1 - y_0} \tag{25}$$

where $y_0 = A_0$. The integral (22) in the deflection angle becomes

$$\phi_f(x_0) = \int_0^1 R(z,x_0) f(z,x_0) dz \tag{26}$$

$$R(z,x_0) = 2\frac{1 - y_0}{A'(x)} P_1(x,x_0) \tag{27}$$

$$f(z,x_0) = P_2(x,x_0) \tag{28}$$

where $x = A^{-1}[(1 - y_0)z + y_0]$.

The function $R(z,x_0)$ is regular for all values of z and x_0, while $f(z,x_0)$ diverges for $z \to 0$. To find out the order of divergence of the integrand, we expand the argument of the square root in $f(z,x_0)$ to the second order in z

$$f(z,x_0) \sim f_0(z,x_0) = \frac{1}{\sqrt{\alpha z + \beta z^2}}. \tag{29}$$

When α is nonzero, the leading order of the divergence in f_0 is $z^{-1/2}$, which can be integrated to give a finite result. When α vanishes, the divergence is z^{-1} which makes the integral diverge. Then the outermost solution of the equation $\alpha = 0$ defines the radius of the photon sphere x_m (see also [18]).

In the case of the Kerr metric, we have

$$\alpha = x_0[x_0(3 - 5x_0 + 2x_0^2) - 2a^2 + 2a\sqrt{a^2 + x_0(x_0 - 1)}] \times [(x_0 - 1)(x_0^3 + a^2(x_0 + 1))]^{-1}. \tag{30}$$

Equation $\alpha = 0$ is equivalent to the third degree equation

$$8a^2 - x_0(3 - 2x_0)^2 = 0. \tag{31}$$

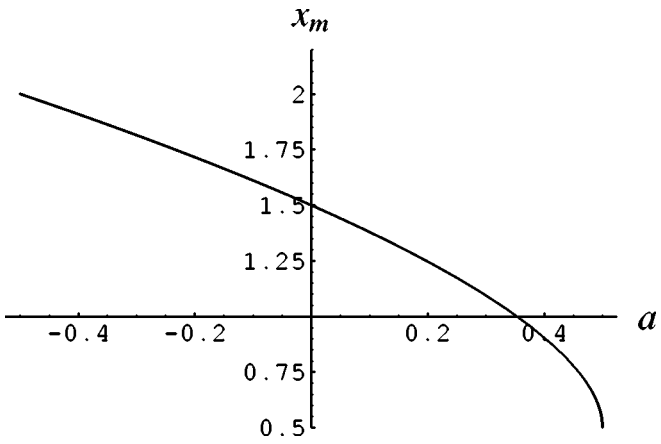

FIG. 2. The radius of the photon sphere versus the black hole angular momentum.

The real solution external to the horizon of this equation defines the radius of the photon sphere x_m, plotted in Fig. 2. As expected, for positive a (direct) photons are allowed to get closer to the black hole, entering even the ergosphere (x_m falls below 1) at high values of a. It is possible to calculate exactly from the equation $\alpha = 0$ at what angular momentum this happens. The critical value is

$$a_{cr} = \frac{1}{2\sqrt{2}} = 0.354. \tag{32}$$

Notice that $x_m \to 1/2$ as $a \to 1/2$, i.e. the photon sphere coincides with the horizon in the limit of extremal Kerr black hole. For negative angular momenta (retrograde) light rays must keep farther from the center.

The procedure to find the strong field limit coefficients is from now on identical to that described in Ref. [11], with $R(z,x_0)$ $f(z,x_0)$ and $f(z,x_0)$ given by Eqs. (27), (28) and (29), respectively. We shall not repeat the whole technique here but just specify the results of Ref. [11] for our metric.

The strong field limit coefficients of the expansion (23) are

$$u_m = \frac{-D_m + \sqrt{4A_m C_m + D_m^2}}{2A_m} \tag{33}$$

$$\bar{a} = \frac{R(0,x_m)}{2\sqrt{\beta_m}} \tag{34}$$

$$\bar{b} = -\pi + b_D + b_R + \bar{a}\log\frac{c x_m^2}{u_m} \tag{35}$$

where

$$b_D = 2\bar{a}\log\frac{2(1 - y_m)}{A'_m x_m} \tag{36}$$

$$b_R = \int_0^1 [R(z,x_m) f(z,x_m) - R(0,x_m) f_0(z,x_m)] dz \tag{37}$$

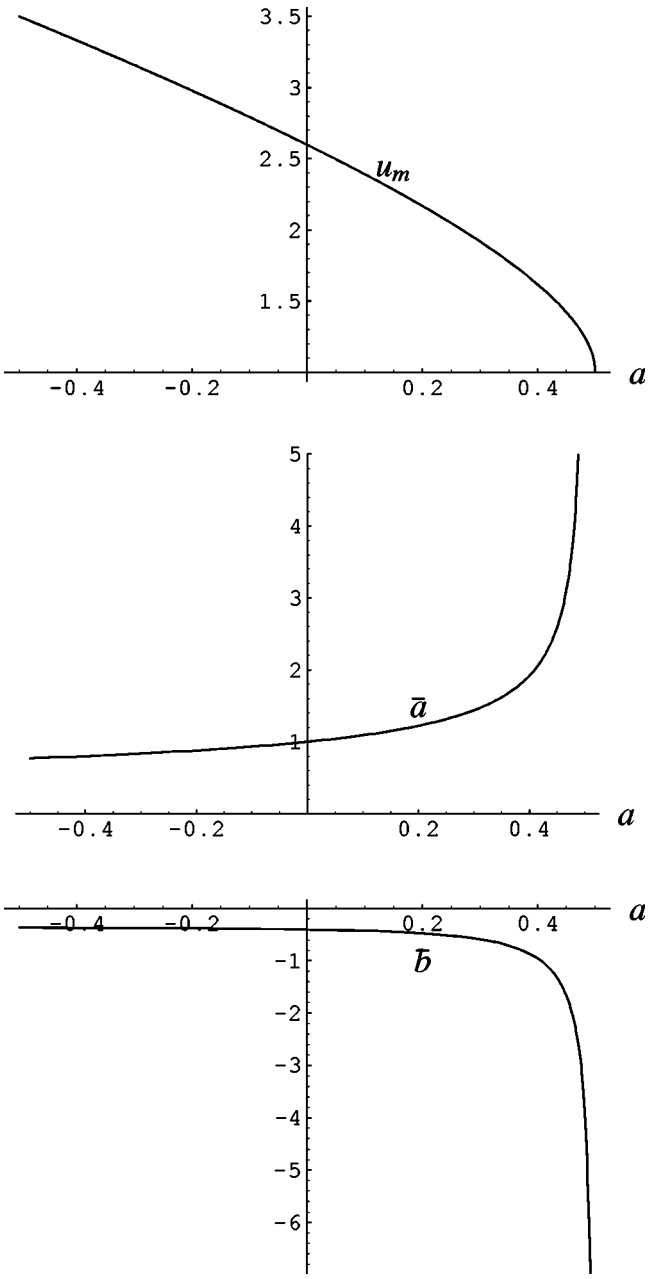

FIG. 3. Coefficients of the strong field limit versus black hole angular momentum.

and c is defined by the expansion

$$u-u_m=c(x_0-x_m)^2. \tag{38}$$

All the functions with the subscript m are evaluated at $x_0=x_m$.

Figure 3 shows the strong field limit coefficients as functions of a. The minimum impact parameter u_m decreases with a in a way similar to x_m. $\bar{a}$ grows and $\bar{b}$ decreases, both diverging with opposite signs at $a=1/2$. The divergence of the coefficients of the expansion warns that the strong field limit deflection angle (23) no longer represents a reliable description in the regime of high a, since x_m becomes a higher order singularity in the function $f(z,x_0)$ and a different expansion should be performed.

IV. PRECESSION OF THE ORBITS AT SMALL DECLINATIONS

The study of the deflection angle for photons lying on the equatorial plane is sufficient to write a one-dimensional lens equation. However, to address the caustic structure and calculate the magnification of the images, we need a two-dimensional lens equation. For this reason, in this section we analyze trajectories close to the equatorial plane. They are described by one further coordinate: the polar angle ϑ, or equivalently, the declination $\psi=(\pi/2)-\vartheta$. The problem becomes too involved to be solved in general but we shall give a complete description for quasi-equatorial motion, preserving also the simplicity and immediacy of the strong field limit scheme.

In order to remain at small declinations, we restrict to light rays characterized by a small inward inclination ψ_0 and small height h compared to the projected impact parameter u, with $\psi_0 \sim h/u$. Retaining the first relevant terms, from Eqs. (13), (14) we get

$$J \simeq u \tag{39}$$

$$Q \simeq h^2+\overline{u^2}\psi_0^2 \tag{40}$$

$$\overline{u} \equiv \sqrt{u^2-a^2}. \tag{41}$$

We require the declination ψ to stay small (of the order of ψ_0) during the motion. Dividing Eq. (12) by Eq. (10), we get a simple evolution equation for ψ as a function of the azimuth ϕ

$$\frac{d\psi}{d\phi}=\pm\,\omega(\phi)\sqrt{\overline{\psi}^2-\psi^2} \tag{42}$$

with

$$\overline{\psi}=\sqrt{\frac{h^2}{\overline{u^2}}+\psi_0^2} \tag{43}$$

$$\omega(\phi)=\overline{u}\frac{a^2+x(\phi)[x(\phi)-1]}{\{a+u[x(\phi)-1]\}x(\phi)}. \tag{44}$$

In the Schwarzschild case ($a=0$), $\omega\to 1$ and Eq. (42) is immediately solved to

$$\psi(\phi)=\overline{\psi}\cos(\phi+\phi_0). \tag{45}$$

After each loop around the black hole, the declination returns to the initial value. This means that there is no precession of the orbital plane, as expected for a spherically symmetric black hole.

For non-vanishing angular momenta, ω is no longer a constant, since x depends on ϕ, and the solution of Eq. (42) is generalized to

$$\psi(\phi)=\overline{\psi}\cos(\overline{\phi}+\phi_0) \tag{46}$$

with

$$\overline{\phi}=\int_0^{\phi}\omega(\phi')d\phi'. \tag{47}$$

Since we are interested in gravitational lensing, the photon comes from infinity and returns to infinity. Therefore, we are interested in the quantity

$$\overline{\phi}_f=\int_0^{\phi_f}\omega(\phi')d\phi', \tag{48}$$

where ϕ_f is the total azimuthal shift experienced by the photon in its whole trajectory, given by Eq. (22).

This integral can be rewritten as

$$\overline{\phi}_f=2\int_{x_0}^{\infty}\omega(x)\frac{d\phi}{dx}dx=\int_0^1 R_\omega(z,x_0)f(z,x_0)dz \tag{49}$$

where

$$R_\omega(z,x_0)=\omega(x)R(z,x_0) \tag{50}$$

with $R(z,x_0)$ and $f(z,x_0)$ given by Eqs. (27) and (28), respectively. At this point, the integral can be solved by the same technique used for the integral (26) with a very similar result. This is possible since $\omega(x)$ adds no singularities and can be englobed in the regular function R.

The final result is

$$\overline{\phi}_f=-\hat{a}\log\left(\frac{\theta D_{OL}}{u_m}-1\right)+\hat{b} \tag{51}$$

$$\hat{a}=\frac{R_\omega(0,x_m)}{2\sqrt{\beta_m}}=1 \tag{52}$$

$$\hat{b}=-\pi+\hat{b}_D+\hat{b}_R+\hat{a}\log\frac{cx_m^2}{u_m} \tag{53}$$

where

$$\hat{b}_D=2\hat{a}\log\frac{2(1-y_m)}{A_m' x_m} \tag{54}$$

$$\hat{b}_R=\int_0^1[R_\omega(z,x_m)f(z,x_m)-R_\omega(0,x_m)f_0(z,x_m)]dz. \tag{55}$$

Notice that the coefficient of the logarithmic term $\hat{a}$ is exactly equal to 1 for all values of the black hole spin. The coefficient $\hat{b}$ is just $\overline{b}+\pi$ in the Schwarzschild limit $a=0$. This recovers the equivalence between the phase in the polar motion $\overline{\phi}_f$ and the total azimuthal shift ϕ_f in this limit. The full behavior of $\hat{b}$ is plotted in Fig. 4. This coefficient diverges as well in the extremal black hole limit $a\to 1/2$.

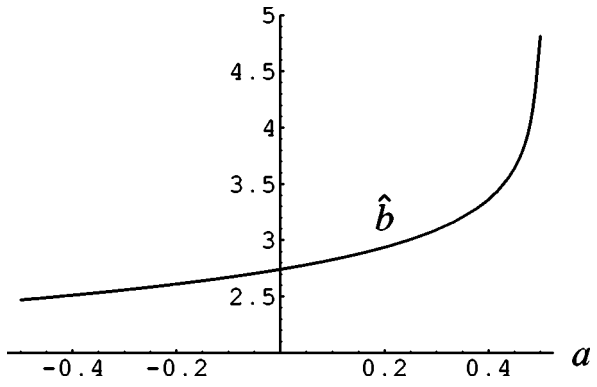

FIG. 4. The coefficient $\hat{b}$ as a function of a.

As a general remark, we can say that for positive angular momenta ω is always less than one, so that $\overline{\phi}_f<\phi_f$. As a consequence, the orbital plane suffers a counterclockwise precession, i.e. after each loop an additional $\Delta\phi$ is necessary to reach the same declination ψ. On the contrary, for negative angular momenta, $\omega>1$. In this case, the precession is clockwise, i.e. the photon reaches the same declination before completing a loop.

The integration constant ϕ_0 in Eq. (46) is fixed by the initial conditions. In particular, we have to impose that at $\phi=0$ the declination is just minus the inclination of the incoming photon trajectory, which we have indicated by ψ_0. The result is that

$$\phi_0=-\,\mathrm{sgn}[h]\arccos\left[-\frac{\psi_0}{\overline{\psi}}\right]. \tag{56}$$

The declination of the outward photon is thus

$$\psi_f\equiv\psi(\phi_f)=\overline{\psi}\cos(\overline{\phi}_f+\phi_0). \tag{57}$$

Alternatively, using the expression of ϕ_0, we can write

$$\psi_f=-\psi_0\cos\overline{\phi}_f-\frac{h}{u}\sin\overline{\phi}_f. \tag{58}$$

The phase $\overline{\phi}_f$, calculated through Eq. (51), has a central importance in the discussion of Secs. VI and VII.

V. LENSING IN THE EQUATORIAL PLANE

In the previous sections we have expressed the deflection angle α as a function of the impact angle θ and the outward declination ψ_f as a function of the incoming inclination ψ_0. We are thus ready to write a lens equation for the Kerr black hole. In this section we shall write the equatorial lens equation, while the next section will deal with the polar lens equation.

So let us start from the ideal case when observer and source both lie on the equatorial plane of the Kerr black hole and the whole trajectory of the photon is confined on the same plane. In previous works, the strong field limit has been developed assuming an almost perfect alignment of source,

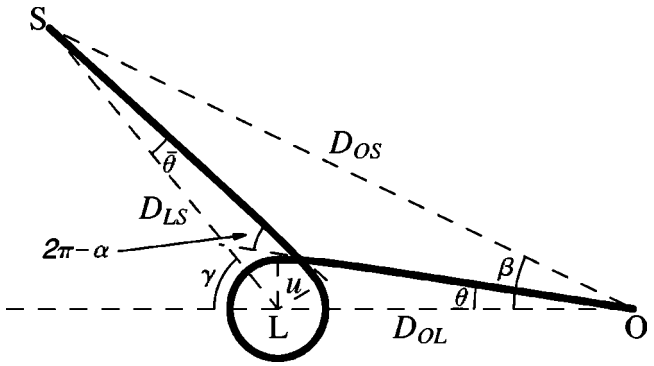

FIG. 5. The lensing geometry projected on the equatorial plane in the case of the first relativistic image. θ is the impact angle as seen by the observer, β is the angular position of the source as seen by the observer, γ is the angular position of the source as seen by the lens, $\bar{\theta}$ is the impact angle from the source.

lens and observer. This is because, for spherically symmetric metrics, the better the alignment the higher is the magnification. As we shall see in Sec. VII, this is no longer the case for Kerr black holes. Therefore we shall write the equatorial lens equation in a more general way, allowing for a generic geometric disposition of lens, source and observer (see Fig. 5).

The optical axis is the line joining the observer and the lens. Setting the origin on the black hole, the angle between the direction of the source and the optical axis will be indicated by γ. $\gamma \simeq 0$ is the case of almost perfect alignment discussed in Refs. [8–11]. From the lensing geometry, illustrated in Fig. 5, we can write the relation

$$\gamma = -\alpha + \theta + \bar{\theta} \bmod 2\pi, \tag{59}$$

where

$$\bar{\theta} \simeq \frac{u}{D_{LS}} \simeq \frac{D_{OL}}{D_{LS}}\theta \tag{60}$$

is the impact angle from the source and D_{LS} is the distance between the lens and the source.

The equatorial lens equation is then

$$\gamma = \frac{D_{OL}+D_{LS}}{D_{LS}}\theta - \alpha(\theta) \mod 2\pi. \tag{61}$$

In this lens equation γ can assume any value in the trigonometric interval $[-\pi, \pi]$. The source may even be on the same side of the observer when $\gamma = \pi$. The relation between γ and β (the angular position of the source as seen by the observer) is

$$\sin\beta = \frac{D_{LS}}{D_{OS}}\sin\gamma, \tag{62}$$

but here in general we cannot substitute the sines by their arguments. D_{OS} is the distance between source and observer which does not coincide with the distance $D_{OL}+D_{LS}$ actually covered by lensed photons.

To solve the lens equation, since $\theta = u/D_{OL} \ll 1$, in a first step we solve the equation $\gamma = -\alpha(\theta) \bmod 2\pi$. Using the expression for the deflection angle derived in the strong field limit (23), we find

$$\theta_n^0 = \frac{u_m}{D_{OL}}(1+e_n) \tag{63}$$

$$e_n = e^{\bar{b}+\gamma-2n\pi/\bar{a}}, \tag{64}$$

where $n = 1,2,\ldots$ indicates the number of loops done by the photon around the black hole. This solution is then corrected expanding $\alpha(\theta)$ around θ_n^0:

$$\alpha(\theta) = \alpha(\theta_n^0) + \left.\frac{\partial\alpha}{\partial\theta}\right|_{\theta_n^0}(\theta-\theta_n^0) + o(\theta-\theta_n^0)$$

$$\simeq -\gamma - \frac{\bar{a}D_{OL}}{u_m e_n}(\theta-\theta_n^0). \tag{65}$$

Substituting in Eq. (61) and neglecting higher order terms, we find

$$\theta_n \simeq \theta_n^0\left(1 - \frac{u_m e_n (D_{OL}+D_{LS})}{\bar{a}D_{OL}D_{LS}}\right), \tag{66}$$

where the correction is much smaller than θ_n^0.

Images are formed on both sides of the lens. As all strong field limit coefficients depend on a we have to be careful and choose the correct sign for the angular momentum. Conventionally we call north the direction of the black hole spin. Then photons winding counterclockwise are direct and are described by a positive a. They form images on the eastern side of the black hole. Images formed by retrograde rays appear on the western side and are described taking a negative a and reversing the sign of γ.

VI. LENSING AT SMALL DECLINATIONS

The lens equation (61) describes trajectories lying on the equatorial plane and can be employed to calculate the positions of the relativistic images. However, to investigate the problem on a deeper level we are forced to study what happens at least for small displacements from the equatorial plane. In this section we shall assist Eq. (61) by its polar counterpart, which is necessary to understand the caustic structure and compute the magnification of the images.

Thanks to the small declination hypothesis, at the lowest order we can neglect any backreaction on the equatorial lens equation. In all our discussion we shall speak (using time reversal) as the photon were emitted by the observer and absorbed by the source.

Consider a source whose height on the equatorial plane is h_S. The height of the observer will be indicated by h_O. We shall assume that the following hierarchy of distances holds (see Fig. 6):

$$u \ll (h_O, h_S) \ll (D_{OL}, D_{LS}). \tag{67}$$

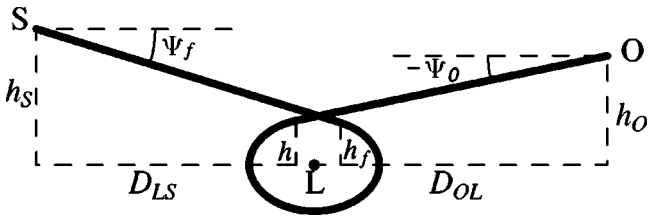

FIG. 6. The lensing geometry projected on the vertical plane. In this picture we have assumed $\gamma=0$ for simplicity.

Recalling the meaning of the parameters ψ_0 and h used insofar to identify the incoming light ray, we can write down the simple geometric relation

$$h=h_O+D_{OL}\psi_0. \tag{68}$$

A similar relation holds between the outgoing photon parameters h_f, ψ_f and the source position

$$h_S=h_f+D_{LS}\psi_f. \tag{69}$$

Given the positions of source and observer, our purpose is to determine ψ_0, the inclination under which the observer emits (sees) the light ray.

By symmetry between the outgoing and the incoming parameters, Eq. (43) for $\bar{\psi}$ can be written substituting ψ_0 and h by ψ_f and h_f

$$\bar{\psi}=\sqrt{\frac{h_f^2}{\bar{u}^2}+\psi_f^2}. \tag{70}$$

In this way, we can express h_f in terms of ψ_f and then, by Eq. (57), in terms of $\bar{\phi}_f$ and ϕ_0

$$h_f=\bar{u}\bar{\psi}\sin(\bar{\phi}_f+\phi_0). \tag{71}$$

Recalling Eq. (56), we also get

$$h_f=-\bar{u}\psi_0\sin\bar{\phi}_f-h\cos\bar{\phi}_f. \tag{72}$$

Substituting in Eq. (69) together with Eq. (58), we get

$$h_S=-\psi_0\bar{u}S-hC-D_{LS}\psi_0C+D_{LS}\frac{h}{\bar{u}}S, \tag{73}$$

where

$$S=\sin\bar{\phi}_f \tag{74}$$

$$C=\cos\bar{\phi}_f. \tag{75}$$

Finally, substituting h from Eq. (68) and discarding higher order terms, we obtain the lens equation in the polar direction

$$h_S=h_O\left(\frac{D_{LS}}{\bar{u}}S-C\right)-\psi_0\left[(D_{OL}+D_{LS})C-\frac{D_{OL}D_{LS}}{\bar{u}}S\right]. \tag{76}$$

In this equation ψ_0 is directly related to the heights of the observer and the source. The solution is

$$\psi_{0,n}=\frac{h_S+h_OC_n-h_O\dfrac{D_{LS}}{\bar{u}}S_n}{-(D_{OL}+D_{LS})C_n+\dfrac{D_{OL}D_{LS}}{\bar{u}}S_n}, \tag{77}$$

where S_n and C_n are S and C calculated for $\bar{\phi}_f=\bar{\phi}_{f,n}$. The phase $\bar{\phi}_{f,n}$ of the nth image is the only quantity that needs to be calculated preliminarly. However, once the equatorial lens equation (61) is solved, we know the impact angle θ_n of the nth image and then we can calculate $\bar{\phi}_f$ by Eq. (51).

As a consistency check we can see what we obtain in the Schwarzschild case when the photon completes just one loop around the black hole, exiting on the opposite side. In this case $a=0$ and $\bar{\phi}_{f,n}=(2n+1)\pi$. We get

$$\psi_{0,n}|_{\bar{\phi}_f=(2n+1)\pi}=\frac{h_S-h_O}{D_{OL}+D_{LS}}, \tag{78}$$

which is the correct result for photons passing very close to the black hole, looping around it.

The consistency of our approximation requires that $\psi_0 \ll 1$ and $h \ll u$. From Eq. (68) the height is

$$h_n=\frac{h_SD_{OL}-h_OD_{LS}C_n}{-(D_{OL}+D_{LS})C_n+\dfrac{D_{OL}D_{LS}}{\bar{u}}S_n}. \tag{79}$$

For a generic $\bar{\phi}_f$, both constraints are automatically satisfied, since the second term in the denominators dominates and we have that $\psi_0 \sim h_O/D_{OL}$ and $h \sim uh_O/D_{OL}$. However, in the neighborhood of $\bar{\phi}_f=k\pi$ the denominators of the two expressions can vanish, making diverge both quantities. The equation

$$K(\gamma)=\bar{u}(D_{OL}+D_{LS})C-D_{OL}D_{LS}S=0 \tag{80}$$

defines the positions of the caustic points. In the next section we will discuss this equation in connection with the magnification of the images formed by sources close to the caustic points (which we call enhanced images for simplicity).

Surprisingly, thanks to the dragging phenomenon, the quasi-equatorial hypothesis is nearly always satisfied, except for enhanced images. In this situation the quasi-equatorial motion hypothesis is satisfied only for particular geometric configurations which keep ψ_0 and h under control.

VII. MAGNIFICATION AND CAUSTIC POINTS

The magnification is classically defined as the ratio of the angular area element of the image and the corresponding angular area element of the source that the observer would see if there were no lens. The angular area element of the image is

$$d^2A_I = d\theta d\psi_0 . \tag{81}$$

The distance covered by the photons is $D_{OL}+D_{LS}$ and then the corresponding angular area element of the source is

$$d^2A_S = \frac{D_{LS} d\gamma dh_S}{(D_{OL}+D_{LS})^2}. \tag{82}$$

In fact the source element in the vertical direction is $dh_S/(D_{OL}+D_{LS})$. In the horizontal direction, the source element is spanned by $d\gamma$ when seen from the lens which corresponds to an angle $D_{LS}d\gamma/(D_{OL}+D_{LS})$ seen from the observer. If we want to compare the luminosity of a lensed image with the luminosity of the direct image (namely the source observed directly along D_{OS} without lensing), the magnification is to be multiplied by the factor $(D_{OL}+D_{LS})^2/D_{OS}^2$.

Our lens application has the form

$$\gamma = \gamma(\theta) \tag{83}$$

$$h_S = h_S(\theta, \psi_0), \tag{84}$$

where the dependence on θ in the polar lens application is through $\bar{\phi}_f$ and we have neglected the backreaction of ψ_0 on γ. The ratio between $d\gamma dh_S$ and $d\theta d\psi_0$ is given by the modulus of the Jacobian determinant of the lens application

$$|J| = \left| \frac{\partial\gamma}{\partial\theta} \frac{\partial h_S}{\partial\psi_0} \right|. \tag{85}$$

The magnification is then given by

$$\mu = \frac{d^2A_I}{d^2A_S} = \frac{(D_{OL}+D_{LS})^2}{D_{LS}} \frac{1}{|J|}. \tag{86}$$

By the equatorial lens equation (61), retaining the dominant terms, we have

$$\frac{\partial\gamma}{\partial\theta} \simeq -\frac{\bar{a} D_{OL}}{u_m e_\gamma}, \tag{87}$$

with

$$e_\gamma = e^{\bar{b}+\gamma/\bar{a}}. \tag{88}$$

In the following, it is convenient to encode the number of loops done by the photon within γ, in order to write more compact formulas for all the relativistic images. So γ can assume any negative real value; γ mod 2π represents the angular position of the source and $n=[(\pi-\gamma)/2\pi]$ is the number of loops done by the photon. Two values of γ differing by a multiple of 2π represent the same source position with respect to the lens, but reached by photons performing a different number of loops around the lens. For example, $\gamma=0$ is a source aligned behind the lens reached by a photon making no loop (weak field lensing); $\gamma=-2\pi$ is the same source behind the lens but reached by a photon making one loop; $\gamma=-4\pi$ is the same source for a photon making two loops, and so on.

By the polar lens equation (76), we have

$$\frac{\partial h_S}{\partial\psi_0} = (D_{OL}+D_{LS})C - \frac{D_{OL}D_{LS}}{\bar{u}} S. \tag{89}$$

Assembling everything together, we get

$$\mu = \frac{(D_{OL}+D_{LS})^2}{D_{OL}D_{LS}} \frac{\bar{u} u_m e_\gamma}{\bar{a}|\bar{u}(D_{OL}+D_{LS})C - D_{OL}D_{LS}S|}. \tag{90}$$

For a generic $\bar{\phi}_f$, $\mu = O(u/D_{OL})^2$, but for the enhanced images, μ may even diverge (formally for point-like sources) when the denominator of Eq. (90) vanishes. The γ's where this happens are called caustic points. At the lowest order in u/D_{OL}, Eq. (80) reduces to

$$\bar{\phi}_f \simeq k\pi. \tag{91}$$

Combining the formula (51) for the phase $\bar{\phi}_f$ with the formula for the deflection angle (23) and using the equatorial lens equation at the lowest order $\gamma=-\alpha(\theta)$, this equation becomes

$$-\frac{\gamma+\bar{b}}{\bar{a}} + \hat{b} = k\pi. \tag{92}$$

The solutions of this equation determine the angular positions γ_k of the caustic points

$$\gamma_k = -\bar{b} + \bar{a}(\hat{b} - k\pi). \tag{93}$$

For each k, we have one caustic point for direct photons and one caustic point for retrograde photons. $k=1$ would describe the weak field caustic points, formed when the azimuthal shift is about π. To be coherent with our strong field limit approximation, we shall restrict our analysis to $k \geqslant 2$.

Expanding the denominator of Eq. (90) around the caustic points, we have

$$K(\gamma) \simeq K'(\gamma_k)[\gamma-\gamma_k(a)] = -\frac{D_{OL}D_{LS}}{\bar{a}}[\gamma-\gamma_k(a)]. \tag{94}$$

To understand the nature of these caustic points, notice that in the Schwarzschild limit $\gamma_k \to -(k-1)\pi$ and all the odd caustic points are aligned on the optical axis behind the lens on consecutive Riemann folds while the even ones are aligned before the lens. If the source is aligned behind the lens, the nth image is given by photons doing n loops around

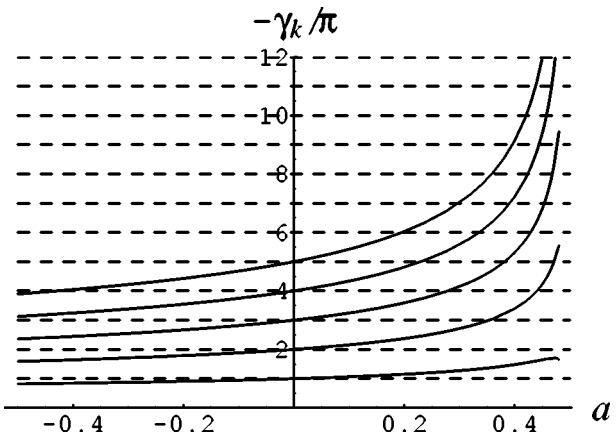

FIG. 7. The angular positions of the first five relativistic caustic points: $k=2,3,4,5,6$ from below to above. When $\gamma=2m\pi$ the source is behind the lens, when $\gamma=(2m+1)\pi$ the source is before the lens.

the black hole. Setting $\gamma\sim-2n\pi$, the closest caustic point is γ_{2n+1}. Then we can recover the Schwarzschild magnification for the images created by a source behind the lens [8]

$$\mu_n^{Sch}=\frac{(D_{OL}+D_{LS})^2}{D_{OL}D_{LS}}\frac{uu_me_n}{\overline{a}\left|\frac{D_{OL}D_{LS}}{\overline{a}}(2n\pi+\gamma)\right|}$$

$$=\frac{D_{OS}}{D_{OL}^2D_{LS}}\frac{u_m^2e_n(1+e_n)}{|\beta|}. \tag{95}$$

In Fig. 7 we plot the positions of the first five relativistic caustic points as functions of the black hole angular momentum. The first relativistic caustic point γ_2 is obtained when the photon turns around the black hole and comes back towards the observer. γ_2 is thus close to $-\pi$ but is anticipated for negative a and delayed for positive a. γ_3 is behind the lens but, at large angular momenta, can move very far from the initial position. At high values of the spin, the caustic points drift so much that they can even change their Riemann fold.

We can specify the magnification formula for the enhanced images using Eq. (94)

$$\mu_k^{enh}=\frac{(D_{OL}+D_{LS})^2}{D_{OL}^2D_{LS}^2}\frac{\overline{\mu_k}(a)}{|\gamma-\gamma_k|} \tag{96}$$

$$\overline{\mu_k}(a)=\overline{u}(\gamma_k(a))u_m(a)e_{\gamma_k(a)}. \tag{97}$$

The quantity $\overline{\mu_k}$ regulates the magnification close to caustic points. The dependence on γ has been extracted and has the typical $|\gamma-\gamma_k|^{-1}$ behavior. The dependence on the astronomical distances D_{OL}, D_{LS}, D_{OS} is negligible in $\overline{\mu_k}$ at the lowest order in u/D_{OL}. So we can use $\overline{\mu_k}$ as a measure

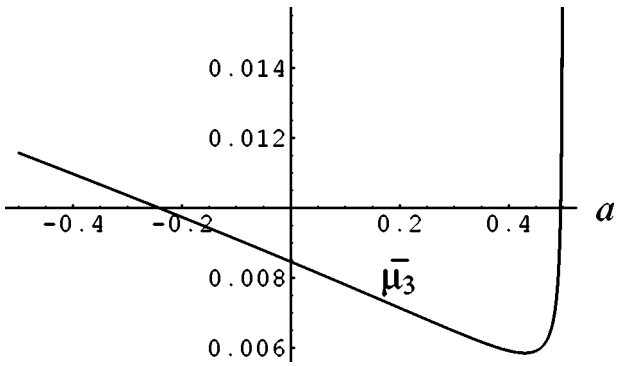

FIG. 8. The magnifying power at the caustic point γ_3.

of the magnifying power of the black hole for different enhanced images and different angular momenta.

In Fig. 8 we plot the magnifying power $\overline{\mu_3}$ of the caustic point γ_3, which for $a=0$ generates the first relativistic image of a source behind the lens. The magnification grows for negative angular momenta while decreases for positive a almost linearly. The divergence in the magnification when a approaches its extremal value 1/2 should not be taken seriously, as the standard strong field limit approximation breaks down as explained in Sec. III.

The shape of $\overline{\mu_k}$ remains more or less the same for every k but, since $e_{\gamma_k}=e^{\hat{b}-k\pi}$, we have that

$$\frac{\mu_{k+1}}{\mu_k}\simeq e^{-\pi}=0.043. \tag{98}$$

The magnification of enhanced images falls quite rapidly as we let the photons make more and more loops.

VIII. CRITICAL CURVES AND CAUSTIC STRUCTURE

It is well known that the Jacobian of the Schwarzschild lens has an infinite series of Einstein rings [3,5]. The first one is the classical weak field Einstein ring whose angular radius is

$$\theta_E=\sqrt{\frac{2D_{LS}}{D_{OL}D_{OS}}}. \tag{99}$$

The corresponding caustic is the point at $\gamma_1=0$.

At small impact parameters we enter the strong field limit of the Schwarzschild lensing and the light rays wind around the black hole. The second Einstein ring is created by photons coming back towards the observer. The caustic is at $\gamma_2=-\pi$.

Decreasing u further, the light ray completes a loop and we have the third Einstein ring, whose caustic point is $\gamma_3=-2\pi$ and is superposed on the first caustic point (on the second Riemann fold).

Summing up, the Schwarzschild lens has a large weak field Einstein ring and an infinite series of concentric relativistic Einstein rings, very close to the minimum impact angle

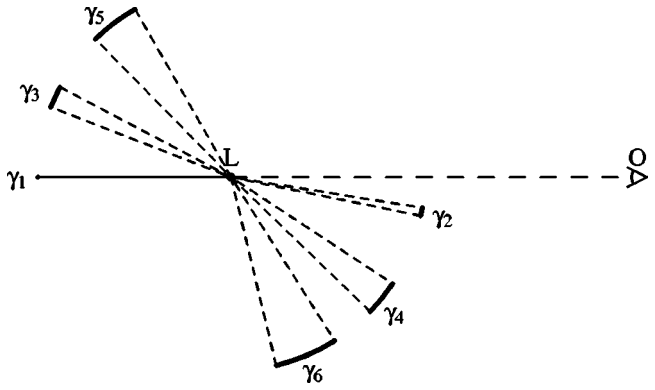

FIG. 9. The first six caustics of the Kerr lens for $a=0.1$, marked by the thick lines between $\gamma_k(-|a|)$ and $\gamma_k(|a|)$.

θ_∞. In the region bounded by the nth ring and the $(n+1)$th ring, the sign of the Jacobian is $(-1)^{n+1}$.

What changes when we turn on the spin of the black hole? As regards the first Einstein ring of the weak field limit, it is distorted and shifted. As a consequence, the caustic point turns into a finite extension diamond shaped caustic [19].

For the critical curves in the strong field limit, we can calculate their intersections with the equatorial plane, which are

$$\theta_k^{cr} \simeq \theta_k^{0,cr}\left(1-\frac{u_m e_{\gamma_k}(D_{OL}+D_{LS})}{\bar{a}D_{OL}D_{LS}}\right) \tag{100}$$

$$\theta_k^{0,cr}=\frac{u_m}{D_{OL}}(1+e_{\gamma_k}). \tag{101}$$

They are closer to the optical axis on the positive a side (for left-winding photons) and farther on the negative a side (i.e. for right-winding photons). Therefore critical curves are distorted and shifted towards the negative a side, which is the western side, if north is the direction of the spin.

The caustics are no longer points but acquire a nonvanishing extension. $\gamma_k(-|a|)$ and $\gamma_k(|a|)$ represent the intersections of the kth caustic with the equatorial plane. As $|\gamma_k(-|a|)|<k\pi$ and $|\gamma_k(|a|)|>k\pi$ the caustic is shifted towards the western side. To visualize this situation, in Fig. 9 we have plotted the projections of the caustics on the equatorial plane, as seen from the north direction. The $[\gamma_1(-|a|),\gamma_1(|a|)]$ caustic is the weak field one, which stays almost aligned on the optical axis, while the relativistic caustics drift in the clockwise direction. As k grows, the caustics become larger and farther from their initial position on the optical axis. Examining Fig. 7 we notice that at high angular momenta the caustics may become very large, covering even several Riemann folds.

At the lowest order in ψ and neglecting any backreaction on the equatorial lens equation it is not possible to give a rigorous classification of the type of catastrophes we encounter on the equatorial plane. However, the fact that the first caustic in the weak field assumes the typical diamond shape of quadrupole lenses suggests a similar picture for strong field caustics. If this is the case, then the caustic points γ_k on the equatorial plane are cusps. This is consistent with the fact that if we let γ decrease below some γ_k the corresponding image changes parity. This can happen only when at the critical point two images are formed with the same parity of the original image [20,21]. These images rapidly move in the vertical direction and are missed in our quasi-equatorial approximation.

IX. PHENOMENOLOGICAL IMPLICATIONS

After all the analysis of the quasi-equatorial lensing in the Kerr spacetime, we are able to discuss the phenomenological relevance of the black hole spin. In Ref. [11] it was shown that all spherically symmetric black holes produce the same patterns of relativistic images. These patterns differ by the separations and the luminosity ratios between different relativistic images. The conclusion was that if strong field gravitational lensing will be caught by future VLBI experiments, it may provide a means to distinguish between different classes of black holes.

In spherically symmetric black hole lensing, a generic source not aligned with the optical axis produces extremely faint relativistic images. On the contrary, a point source perfectly aligned along the optical axis produces (theoretically) infinitely bright images. Actually the finite source radius cuts off the real brightness of the images. The relativistic images are maximally amplified altogether since all the caustic points of spherically symmetric black holes lie on the optical axis.

In Kerr lensing, the situation becomes radically different. The crucial fact is that the caustics no longer lie on the optical axis but drift throughout the trigonometric interval. Then if the source is close to one caustic point, it cannot be close to any other. The consequence is that only one image at a time can be enhanced, while all the others stay extremely faint.

To clarify the situation, suppose we have a source aligned with the caustic point $\gamma_3(|a|)$. Then the outermost relativistic image on the eastern side will be enhanced. If we put the source on $\gamma_3(-|a|)$, then we only enhance the first relativistic image on the western side. If we put the source on $\gamma_5(|a|)$, then the second relativistic image on the eastern side will be enhanced and so on.

Rather than seeing an infinite series of relativistic images on each side of the lens, we would observe only one enhanced relativistic image. It would be difficult to recognize a single image as a gravitational lensing phenomenon rather than any kind of environmental source around the black hole. Even if we managed, it would be quite tricky to extract information about the strong fields around the black hole from one single relativistic image.

However, if the source is inside the caustic, two additional images should appear, making it easier to recognize their real nature of lensed images of the same source. Moreover, three images can be used to investigate the gravitational field around the black hole and put constraints on its parameters. Alas, the additional images are missed in our quasiequatorial approximation. In order to catch them, it is

necessary to face the problem of Kerr lensing in its general form. A reliable treatment of non-equatorial images would complete our quasi-equatorial study and would make possible a detailed investigation of strong field gravitational lensing for high values of the black hole spin.

By now, we have discussed the two extreme situations: spherically symmetric black holes ($a=0$) and high spin black holes. It is interesting to estimate the value of the spin which separates the two regimes. We shall do it, referring to the black hole at the center of our Galaxy, assuming $D_{OL}=8.5$ kpc, $D_{LS}=1$ kpc.

In order to consider a black hole as spherically symmetric, the caustic drift must be negligible when compared to the extension of the source. In fact, in this case, the source does not ''see'' different caustics but they behave roughly as if they were all at the same point. For small a the γ_k scale linearly as $-(k-1)\pi-a(\eta_0+\eta_1 k)$, with η_0 and η_1 numerical factors of order one. Then, the drift between two consecutive caustics will be negligible if

$$|\gamma_k(a)-\gamma_{k+2}(a) \mod 2\pi| = 2\eta_1 a \ll \frac{R_S}{D_{LS}}. \quad (102)$$

If we consider a source with radius $R_S=10R_\odot$, we then find that a should be lower than 10^{-10}. When a is greater than this value, the source will see only one caustic at a time. However, the caustic will be still seen as point-like, since the extension of the caustic scales as a^2. Therefore, we will still have two enhanced images, corresponding to the two intersections of the kth caustic with the equatorial plane $\gamma_k(a)$ and $\gamma_k(-a)$. This intermediate situation takes place as long as

$$|\gamma_k(a)+(k-1)\pi|-|\gamma_k(-a)+(k-1)\pi| = (\xi_0+\xi_1 k)a^2 \ll \frac{R_S}{D_{LS}} \quad (103)$$

with ξ_0 and ξ_1 of order one.

For a $10R_\odot$ source, this requires $a \ll 10^{-5}$. Beyond this value, only one image at a time will be enhanced (together with an eventual additional pair of images if the source is inside the caustic), while all the others stay invisible.

These estimates reveal that the phenomenology of spherically symmetric black holes is realistic only for black holes with tiny spin. Yet, as recalled in the Introduction, the first estimates of the spin of the black hole at the center of our Galaxy push towards high values [14]. If these estimates are confirmed, then we are forced to include spin in any realistic treatment of strong field gravitational lensing for Sgr A*.

X. SUMMARY

In this paper we have explored the modifications to strong field limit gravitational lensing induced by the rotation of the central body, analyzing the quasi-equatorial null geodesics.

The most apparent change is the formation of extended caustics which, for high angular momenta, can cover several Riemann folds. This situation is radically different from spherically symmetric black holes where the caustics are points aligned behind and in front of the lens. While for $a=0$ a source behind the lens is simultaneously close to all odd caustics and gives rise only to enhanced images, for Kerr black holes the source can be close to one caustic at a time and thus produces only one enhanced image.

As secondary interesting effects, we can also mention the asymmetry between images formed by photons winding in the same sense of the black hole and photons winding in the opposite sense, the latter appearing farther from the black hole. The magnification decreases with the spin, being higher for retrograde images.

The study of quasi-equatorial Kerr gravitational lensing is very instructive and has allowed us to discover a great number of interesting features of spinning black holes. However, to address the phenomenology of the black hole at the center of our Galaxy and/or other black holes with deeper insight, further investigation is necessary. In fact, we need a punctual description of the caustic structure not limited to the equatorial plane. The existence of extended caustics suggests the formation of pairs of non-equatorial images, missed in our approximation, which are of striking importance for the phenomenology.

The quasi-equatorial lensing, studied in this work, then represents the first fundamental step to understanding lensing by spinning black holes. However, the complexity of the problem requires a global approach in order to give correct and complete answers to all observational questions. This is the main objective for future work on strong field gravitational lensing.

ACKNOWLEDGMENT

I am grateful to Mauro Sereno for useful discussions on the subject.

[1] J.M. Bardeen, *Black Holes*, edited by C. de Witt and B.S. de Witt (Gordon & Breach, New York, 1973), p. 215.
[2] S.U. Viergutz, Astron. Astrophys. **272**, 355 (1993).
[3] R.J. Nemiroff, Am. J. Phys. **61**, 619 (1993).
[4] H. Falcke, F. Melia, and E. Agol, Astrophys. J. Lett. **528**, L13 (1999).
[5] K.S. Virbhadra and G.F.R. Ellis, Phys. Rev. D **62**, 084003 (2000).
[6] S. Frittelli, T.P. Kling, and E.T. Newman, Phys. Rev. D **61**, 064021 (2000).
[7] K.S. Virbhadra and G.F.R. Ellis, Phys. Rev. D **65**, 103004 (2002).
[8] V. Bozza, S. Capozziello, G. Iovane, and G. Scarpetta, Gen. Relativ. Gravit. **33**, 1535 (2001).
[9] E.F. Eiroa, G.E. Romero, and D.F. Torres, Phys. Rev. D **66**, 024010 (2002).

[10] A.O. Petters, Mon. Not. R. Astron. Soc. **338**, 457 (2003).
[11] V. Bozza, Phys. Rev. D **66**, 103001 (2002).
[12] ARISE web page: arise.jpl.nasa.gov; MAXIM web page: maxim.gsfc.nasa.gov; J.S. Ulvestad, astro-ph/9901374.
[13] D. Richstone *et al.*, Nature (London) **395**, A14 (1998).
[14] S. Liu and F. Melia, Astrophys. J. Lett. **573**, L23 (2002).
[15] R.H. Boyer and R.W. Lindquist, J. Math. Phys. **8**, 265 (1967).
[16] B. Carter, Phys. Rev. **174**, 1559 (1968).
[17] S.W. Hawking and G.F. Ellis, *The Large Scale Structure of Space-time* (Cambridge University Press, Cambridge, England, 1973).
[18] C.-M. Claudel, K.S. Virbhadra, and G.F.R. Ellis, J. Math. Phys. **42**, 818 (2001).
[19] M. Sereno (in preparation).
[20] P. Schneider and A. Weiß, Astron. Astrophys. **260**, 1 (1992).
[21] S.H. Rhie, astro-ph/0207612.